Basement controls on deformation during oblique convergence: Transpressive structures in the western Qaidam Basin, northern Tibetan Plateau

Runchao Liu[1], M. B. Allen[2], Qiquan Zhang[3], Wei Du[1], Xiang Cheng[1], R. E. Holdsworth[2], and Zhaojie Guo[1*]

[1]*Key Laboratory of Orogenic Belts and Crustal Evolution, Ministry of Education, School of Earth and Space Sciences, Peking University, Beijing 100871, China*

[2]*Department of Earth Sciences, University of Durham, Durham DH1 3LE, UK*

[3]*Qinghai Oilfield Company, Petrochina, Dunhuang, Gansu 736202, China*

ABSTRACT

The Qaidam Basin, especially its western part, is characterized by numerous NW-trending folds and faults. Understanding the style and formation mechanism of these structures is crucial for unravelling the deformation of the Qaidam basin, and the broader tectonics of the northern part of the Tibetan Plateau. Based on seismic data, we reconstruct the structural framework of the central part of the western Qaidam Basin, and find that: (1) the structures in this area display positive flower geometries in 2D seismic profiles and helicoidal shapes in 3D space; (2) these positive flower structures began to develop during the middle to late Miocene (15-8 Ma); (3) these positive flower structures are controlled by left-lateral basement faults and formed in a random temporal sequence. The left-lateral features represent the strike-slip component of distributed deformation, consistent with published GPS and seismicity data for oblique convergence across the north of the Tibetan Plateau.

Collectively, they perform the same role as the discrete Haiyuan, Kunlun and Altyn Tagh faults in adjacent areas.

INTRODUCTION

The formation and deformation of the Qaidam Basin was, along with the uplift and growth of the Tibetan Plateau, due to the collision of India with Eurasia (Argand, 1924; Molnar and Tapponnier, 1975) during the past ~50 million years (Patriat and Achache, 1984; Garzanti et al., 1987; Rowley, 1996; Huang et al., 2015). However, in contrast to the surrounding mountains in the northeastern Tibetan Plateau (Fig. 1; Dupont-Nivet et al, 2004; Duvall and Clark, 2010; Wang et al., 2011; Zheng et al., 2013), the Qaidam Basin is known to have a relatively rigid, possibly cratonic basement (Zhu and Helmberger, 1998; Shen et al., 2001; Yuan et al., 2013; Yu et al., 2014). How the Qaidam Basin deforms in the context of the higher regions of the Tibetan Plateau has been of interest to many geologists (England and Molnar, 1997; Royden et al., 1997; Dayem et al., 2009).

Some workers put emphasis on N-S compression and shortening of the Qaidam Basin, and tend to interpret the Cenozoic structures within the basin as thrust-fault related folds (Métivier et al., 1998; Chen et al., 1999; Yin et al., 2007, 2008a; Meng and Fang, 2008). The strike-slip component to the deformation, if any, is less clear. Certainly, the active deformation across the whole northeastern Tibetan Plateau involves oblique convergence: GPS vectors with respect to stable Eurasia are oriented oblique to the regional fault and fold traces (e.g. Gan et al., 2007; Fig. 1). However, whilst strain partitioning (i.e. the spatial separation of deformation caused by oblique

convergence into dip-slip and strike-slip components) to the north and south of the Qaidam Basin takes place via strike-slip localization on single faults (Haiyuan and Eastern Kunlun), it is not clear what happens within the basin interior, and how the oblique convergence ("transpression") is actually expressed. As an additional factor in the regional tectonics, Meyer et al. (1998) and Pan et al. (2015) suggested that structures within the Qaidam Basin are splays from the Altyn Tagh Fault, which can extend up to 400 km away.

In this paper, we analyse 2D and 3D seismic data over a series of anticlines in the western part of the Qaidam Basin, to investigate the subsurface structural framework of this region. We propose a new interpretation of the structural styles in the western Qaidam Basin, with broader implications for the deformation mechanism and tectonic evolution of this part of the Tibetan Plateau.

GEOLOGICAL SETTING AND STUDY AREA

The Qaidam Basin, with sedimentary cover of c.120,000 km², is the largest Cenozoic intermontane basin in the northeastern Tibetan Plateau, bounded by the Qimen Tagh-Eastern Kunlun mountain belts to the south, the Altyn Tagh mountain belts to the northwest and the Qilian Shan-Nan Shan mountain belts to the north (Fig. 1; Métivier et al., 1998; Zhai et al., 2002; Wang et al., 2006). The relatively low elevation (~3000 m) and limited deformation of the Qaidam Basin, compared to the strongly deformed surrounding mountain belts, is attributed to the higher strength of the its underlying crust relative to the surrounding regions. Geophysical explorations (Zhu et al., 1995; Jordan and Watts, 2005; Zhao et al., 2006, 2013; Li et al., 2013) and

geological investigations (Zhai et al., 2002; Wang et al., 2004; Hao et al., 2004; Yu et al., 2014) have demonstrated that the Qaidam Basin has a Precambrian crystalline basement with high effective elastic thickness. Benefitting from hydrocarbon exploration since 1954, the integrated chronostratigraphic, lithostratigraphic and seismic stratigraphic framework of the Qaidam Basin has been established (Fig. 2b; Sun et al., 2007). The Qaidam Basin is mainly filled with Cenozoic non-marine deposits except in some places along the Qilian Shan-Nan Shan and the Altyn Tagh, which are underlain by Mesozoic sequences (Jurassic-Lower Cretaceous) (Ritts and Biffi, 2000; Jin et al., 2004; Xu et al., 2006). The Cenozoic strata of the Qaidam Basin are divided into eight lithostratigraphic units, each of which has been dated precisely based on paleontology and magnetostratigraphy studies (Gu et al., 1990; QBGMR, 1991; Yang et al., 1992; Sun et al., 2002; Sun et al., 2005; Fang et al., 2007; Lu and Xiong, 2009; Pei et al., 2009; Zhang et al., 2013; Ke et al., 2013). They are: (1) the Lulehe Formation (E_{1+2}l), >53.5-43.8 Ma; (2) the Lower Xiaganchaigou Formation (E_3^1xg), 43.8-37.8 Ma; (3) the Upper Xiaganchaigou Formation (E_3^2xg), 37.8-35.5 Ma; (4) the Shangganchaigou Formation (N_1sg), 35.5-22.0 Ma; (5) the Xiayoushashan Formation (N_2^1xy), 22.0-15.3 Ma; (6) the Shangyoushashan Formation (N_2^2sy), 15.3 -8.1 Ma; (7) the Shizigou Formation (N_2^3s), 8.1-2.5 Ma; (8) the Qigequan Formation (Q_1q), 2.5-0.01 Ma (Fig. 2b).

The crustal deformation of the Qaidam Basin is mainly concentrated in its western part (Zhou et al., 2006; Yin et al., 2008b), where numerous NW-trending faults and folds are oriented at high angles to the Altyn Tagh fault (Fig. 1; Sun et al.,

1956; Song and Wang, 1993; Ge et al., 1998; Yin and Harrison, 2000). The study area in this paper is located in the central part of the western Qaidam Basin, between the Yingxiongling structure belts (to the south) and the Eboliang structure belts (to the north). Both the geological map (Fig. 2a) and the digital elevation model (DEM, Fig. 4) show a series of periclines (3≤length-width ratio≤10) in the study area, arranged in en-echelon patterns. These anticlines are located far from the basin boundaries and display slightly sigmoidal traces (lazy Z-shaped).They are the key to understanding the structural deformation pattern within the western Qaidam Basin. The exposed strata in the study area range from Eocene to Holocene in age (Fig. 2a).

DATA AND METHODS

The analyses of the structural style and the reconstruction of the subsurface fault system within the study area are primarily based on seismic data provided by the Qinghai Oilfield Company (China). We selected forty-one 2D seismic profiles and two 3D seismic datasets that cover most anticlines in the central region of the western Qaidam Basin with an area of c. 4200 km^2 (Fig. 2a). The original seismic data, pre-stack time migration SEGY files, were integrated into and interpreted by the commercial software, Kingdom (HIS). The 2D seismic profiles consist of 39 inlines (SW-NE) and 3 crosslines (NW-SE) with maximum recording times of 6 s or 7 s two-way time (TWT) for different batches of profiles (from the 1980s to the 2000s). The TWT extends down to 6 s and 5 s for the two 3D seismic datasets, Xiaoliangshan (2011) and Nanyishan (2008), respectively. Average inline spacing is 2 km for both the 2D seismic profiles and 3D seismic datasets, which is tight enough to detect subtle

111 structural changes along the strike of a single anticline. The three relatively long 2D
112 seismic crosslines were linked up one by one, crossing all the 2D seismic inlines and
113 the two 3D seismic datasets, and were mainly used for closing the same seismic
114 reflection horizons and faults.

115 The seismic reflection boundaries between the sedimentary cover and basement,
116 between the Cenozoic and the Mesozoic, and between the adjacent Cenozoic
117 formations are recognized throughout the entire basin and are termed T_6, T_R, T_5, T_4, T_3,
118 T_2', T_2, T_1 and T_0 (from bottom to top) (Fig. 2b; Xu et al., 2004). In our work, the
119 calibration of each seismic stratigraphic horizon (T_0-T_6) was constrained precisely by
120 synthetic seismograms and substantiated by borehole records, followed by lateral
121 comparison and tracking. The depiction of the faults was strictly based on the offset of
122 seismic events in the sedimentary cover and was inferred in the basement. However,
123 the down-dip continuation of faults kept a uniform pattern from the shallow
124 sedimentary layers to the deep basement. After interpreting all the selected seismic
125 sections (e.g. Fig. 3), we delineated the reliable 3D geometry of the underground
126 structures (e.g. Fig. 4b). Furthermore, the fault intersection points on each seismic
127 stratigraphic horizon were projected to the surface (digital elevation model, DEM),
128 making up the fault system distribution map. Planimetric positions of the shallowest
129 piercing points of the faults with significant vertical offsets were compared with the
130 topography (morphological scarps) (Fig. 4a).

131 ## OBSERVATIONS AND INTERPRETATION

132 This section presents seismic reflection data and other evidence (geomorphology,

and depth-structure maps) which were used to reconstruct the structural framework of the study area.

Geometry of the Subsurface Faults and Anticlines

The major structural elements depicted in the seismic sections crossing the study area (SW-NE) are a series of positive flower structures, with growth strata ranging from middle to late Miocene (Fig. 3). Although the general shapes of the flower structures are similar through all inline sections, comparison of these sections shows significant differences with respect to number, arrangement and preferred dip directions of branch faults within each of the flower structure (see below). Observed differences also include the occurrence of syntectonic strata and the depth of branch lines of the major faults.

The southwest-vergent Xiaoliangshan anticline in section A-A' (Fig. 3a) is bounded by two steep faults zones (>60°) and has a curved crest. Between the two boundary faults zones, there are several minor branch faults which also help to form the uplifted core of the Xiaoliangshan anticline. The gentle limbs of the Xiaoliangshan anticline display a wide interlimb angle (>120°). The almost flat strata outside the two main branch faults indicate that folding deformation is confined by the flower structure with a width of ca. 7 km. The two wide boundary fault zones are characterized by chaotic seismic reflections and fault plane reflections. They intersect near the base of the sedimentary cover sequence and combine into one major SW-dipping fault extending down into the deeper basement. The trace and dip of the basement fault are inferred from the differential uplift of the fault-blocks and the

opposite dip directions of the seismic reflections in the basement on either side of the major fault, respectively. The T_1 seismic reflector (~8.1 Ma) is the boundary between the pre-growth strata and the growth strata of the Xiaoliangshan anticline, below which the thickness of each stratigraphic unit keeps constant across the flower structure, and above which the strata thicken towards the anticline flanks and the outside of the boundary faults.

In section B-B' (Fig. 3b), the Nanyishan anticline is a symmetrical, arcuate fold with a wide interlimb angle (>120°), which is also characterized by a positive flower structure with a width of ca. 10 km. A detachment zone (at ca. 3.3s TWT) composed of dark mudstones in the Middle Eocene Lower Xiaganchaigou Formation (Wang, 2003) separates the major fault below from the branch faults above. The steep NE-dipping major fault (>65°) extends from the basement up to the detachment zone, and can be traced in the same way used in the Xiaoliangshan anticline. Above the detachment unit, numerous small branch faults define two wide boundary fault zones (>55°), while few branch faults develop between these two fault zones. Growth strata in the Nanyishan anticline occur above the T_1 seismic reflector. The southeastern end of the Xiaoliangshan anticline, as shown in section B-B', is defined by only two single branch faults that reach the T_2'seismic reflector with minor fault throw and fold deformation.

In section C-C' (Fig. 3c), the limbs of the Jiandingshan anticline are asymmetric showing a northeast vergence, with a half-wavelength of ca. 11 km. The steep basement-involved major fault branches upwards into three narrow faults (>65°)

177 bounding the anticline, with the largest throw along the northeastern boundary. The
178 branch points of the Jiandingshan flower structure are at greater depths, far below the
179 T_6 seismic reflector, compared to those of the Xiaoliangshan and the Nanyishan
180 flower structures. The strata above T_2'seismic reflector (~15.3 Ma) in this section
181 show an obvious trend of thickening from the anticline high-point to the flanks, and
182 represent the growth strata of the Jiandingshan anticline. An anomalous E-W striking,
183 NNE-dipping fault to the south does not seem to be related to the Jiandingshan flower
184 structure (Fig. 4a).
185 Section D-D' (Fig. 3d) crosses the Dafengshan, the Heiliangzi and the Jianbei
186 anticlines. The western segment of the Dafengshan anticline has a simple geometry,
187 with an upright, gentle crest confined by two boundary faults (>65°). These two main
188 branch faults may intersect with each other at a deeper level than 6s TWT. The growth
189 strata of the Dafengshan anticline occur above the T_2' seismic reflector. The
190 Heiliangzi anticline in this section behaves as an asymmetric positive flower structure
191 with a northeastward throw, due to a significant reverse-slip component along its
192 northeastern boundary branch fault (>65°). It succeeds the geometry of the
193 Jiandingshan anticline southeasterly (Fig. 2). Growth strata of the Heiliangzi anticline
194 occur after T_1 which is a little later than that of the Jiandingshan anticline (T_2'). The
195 Jianbei anticline, located on the north of the Heiliangzi anticline, has a similar
196 geometry to the Heiliangzi anticlines, and its growth strata occur above the T_2'
197 seismic reflector.
198 Section E-E' (Fig. 3e) crosses the Dafengshan, the Heiliangzi and the

Changweiliang anticlines. The Changweiliang anticline is the southeastern continuation of the Jianbei anticline (Fig. 2). Compared with section D-D', the three anticlines in section E-E' are more upright and symmetric, whilst the fault system of the Dafengshan flower structure has more branch faults, and the northeastern boundary faults of the Heiliangzi and the Changweiliang flower structures become less important whilst the southwestern boundary faults have a great impact on their geometry. The branch lines of the three flower structures in section E-E' occur near the T_6 seismic reflector and are possibly influenced by Mesozoic strata with half-graben sedimentary geometry. Section F-F' (Fig. 3f) shows the geometry of the southeastern segment of the Dafengshan anticline and the middle segment of the Jianshan anticline. In this section, the positive flower geometry of these two anticlines is clear, with one being asymmetric and tilting toward the southwest while the other is symmetric. The growth strata of the Jianshan anticline developed above the T_2' seismic reflector.

In addition to the differences among the anticlines described above, the subsurface geometry of each anticline changes gradually along strike. For instance, the Dafengshan anticline shows a ribbon effect in the three-dimensional space (Fig. 4b; Zolnai, 1991). The western part of the Dafengshan anticline is asymmetric and verges to the northeast, and the major fault in the basement dips to the southwest (e.g. seismic lines Ⅰ, Ⅱ and Ⅲ in Fig. 4b). The middle part of the Dafengshan anticline turns symmetric and the major fault cuts into the basement almost vertically (e.g. seismic lines Ⅳ and Ⅴ in Fig. 4b). The eastern part of the Dafengshan

anticline becomes asymmetric again, but the dip directions of the fold axial plane and the major basement fault are of opposite polarity to those in the western part (e.g. seismic lines Ⅵ and Ⅶ in Fig. 4b). The fold amplitude, the number of branch faults, the offset of each branch fault and the depth of branch lines at the western and eastern ends of the Dafengshan anticline are gentler, less, smaller and deeper than those at the middle part of the Dafengshan anticline, respectively. These changes reveal the differential deformation magnitude along the strike of the Dafengshan anticline.

Distribution of the Faults and Anticlines in Map View

The fault traces mapped on the T_1, T_2', T_2, T_4 and T_6 seismic stratigraphic horizons were projected to the surface. These fault traces lie sub-parallel to the curved traces of the anticline boundaries, but in detail cross the anticline axes at very low angles (<5°) (Fig. 4a). The anticline axes have a slightly sigmoidal appearance (lazy Z-shaped) in the plan view whereas the fault traces are straighter and more segmented. The dominant set of faults has an average strike of N130°E, and the minor set has only four short faults with an average strike of N95°E (Fig. 4a, inset). These minor faults are P shears to the dominant set. The dominant faults form the branch faults of the positive flower structures. Some of them converge at one place and diverge at another place along the strike (e.g. the Xiaoliangshan and the Dafengshan anticlines), and adjacent branch faults of one flower structure may propagate displacement sideways (e.g. the Jiandingshan, the Heiliangzi and the Jianbei anticlines) (Fig. 4a).

The morphological scarps on the each side of the anticlines are the surface expression of the boundary branch faults, and their development is also affected by

the northwesterly wind erosion in the Qaidam Basin (Kapp et al., 2011; Wu et al., 2014a). The largest scarps coincide with the underlying faults which exhibit considerable vertical offsets and are preserved on the leeward side of the anticlines, such as the southern boundary scarps at the middle segments of the Xiaoliangshan and the Nanyishan anticlines (Fig. 4a). A typical horsetail feature controlled by near-surface splay faults can also be found at the eastern end of the Dafengshan anticline (Fig. 4a).

Sinistral Faulting along the Structures

Depth-structure maps are basic tools in hydrocarbon exploration because they play a useful role in deploying wells and calculating closures and areas of traps. Such depth-structure maps can also contain useful information about the geometry and causative kinematic processes of folds (Rickard, 1971; Shaw et al., 1994). Based on plentiful seismic profiles and dense time-depth conversion data, depth-structure maps of every seismic horizon (T_0-T_6) in the western Qaidam Basin were compiled by the geoscientists of Qinghai Oilfield Company.

T_2 depth-structure maps of the Jiandingshan, Nanyishan and Dafengshan anticlines are shown as examples (Fig. 5). The 1600 meter depth contours of are chosen as a reference in the Jiandingshan area (Fig. 5a). The foot-wall of the Northern Jiandingshan Fault (NJF) is offset to the northwest relative to the hanging-wall, which indicates sinistral strike-slip component on the Northern Jiandingshan Fault. Sinistral movements are also observed on the Northern Nanyishan Fault (NNF in Fig. 5b) and the Southern Dafengshan Fault (SDF in Fig. 5c). Using gradients of the dipping strata

and distances between the endpoints of the reference contour lines from the depth-structure maps, the vertical and lateral offsets are calculated for these three steep faults (Table.1; Figs. 3b, 3c and 3e; Maltman, 1998). The results reveal that the vertical offsets are much smaller than the sinistral offsets; the former range from 0.2 to 0.6 km, while the latter range from 1.0 to 3.5 km.

DISCUSSION

Is the Western Qaidam Basin Dominated by Contractional or Transpressive Structures?

At early stages of hydrocarbon exploration in the Qaidam Basin, the anticlines in the western part of the basin were identified as a series of uplifted folds, each of which was thought to be bounded by two oppositely dipping reverse faults (Gu et al., 1990). This interpretation was based on undulations and offsets of the seismic reflectors without much consideration of the formation mechanism. Xia et al. (2001) and Zhai et al. (2002) followed this interpretation scheme and proposed that the boundary faults are inverted normal faults. However, structures with normal faults are primarily located in Jurassic strata along the northern margin of the Qaidam Basin and the Altyn Tagh piedmont (Zeng et al., 2002; Wu et al., 2006; Fu et al., 2015), with rare stratigraphic evidence for Paleogene normal faults (Jin et al., 2004; Yin et al., 2008b). The only evidence for Jurassic normal faulting in the study area lies to the north of the eastern segment of the Dafengshan anticline (Fig. 3, sections E-E’ and F-F’).

An alternative explanation (e.g. Zhou et al., 2006; Yin et al., 2008b; Wu et al., 2014b) follows a fold-and-thrust belt model, interpreting the structures in the western

Qaidam Basin as Jura-type folds which develop in the distal region of a foreland thrust belt (Wang et al., 2012; Yu et al., 2016). Structural styles in this tectonic model include fault-propagation folds, fault-bend folds, detachment folds, conjugate kink-band zones and structural wedges (Zheng et al., 2007; Liu et al., 2009; Xu et al., 2013; Wu et al., 2014a). However, this interpretation scheme is challenged by the seismic data presented here, for the following reasons: (1) the boundary faults of most anticlines in the western Qaidam Basin are much steeper (>55°; Fig. 3) than the theoretical thrust faults under horizontal compressive stress; (2) the folded strata are confined between the boundary faults of each anticline and generate large interlimb angles (Figs. 3 and 4); (3) the southern and northern tectonic boundaries of the Qaidam Basin are dominated by high angle basement steps with considerable lateral displacements, making the development of a single ubiquitous decollement unlikely (Wei et al., 2005; Wang et al., 2008; Cheng et al., 2014; Cheng et al., 2015).

In this study, we have identified several anticlines in the western Qaidam Basin that are linked to positive flower structures, with branch faults that consistently converge at the tops of the principle displacement zones (PDZ) of the major faults (Fig. 3; Beidinger and Decker, 2011). The surface appearances of these helicoidal flower structures are laterally-propagating boundary faults and S-shaped fold traces, which indicate sinistral strike-slip motion along the major basement faults (Fig. 4a, b). The left-lateral displacement magnitudes of these faults can be determined by the depth-structure maps of anticlines (e.g. Table.1; Fig. 5). The kinematic characteristics of surface minor fractures around the anticlines in the study area also indicate

left-lateral transpressive deformation (e.g. Fig. 6), which means an opposite slip direction on the same faults to that deduced by Mao et al. (2016). Thus, we propose that the dominant structures in the western Qaidam Basin are a series of discrete positive flower structures controlled by left-lateral transpressive faults which root downwards into the basement (Sylvester, 1988; Harding, 1990; Woodcock and Rickards, 2003) (Fig. 7a). We do not exclude the possibility that detachment movements of different magnitudes may take place in the ductile sedimentary layers of some structures in this region, such as the Nanyinshan and Shizigou-Youshashan anticlines (Wang, 2003; Yu et al., 2011; Wu et al., 2014a).

Timing of Deformation

Cenozoic sedimentation and deformation in the Qaidam Basin initiated within 10 Myr of the initial Indo-Eurasia collision (Yin et al., 2002; Yin et al. 2008a) indicating that the far-field effects of continental collision were rapidly transferred to the northern part of the Tibetan Plateau. The resultant uplift of the Qilian Shan-Nan Shan range and sinistral strike-slip movement along the Altyn Tagh Fault configured the initial northern and northwestern boundaries of the Qaidam Basin, respectively (Yin et al., 2002; Zhou et al., 2006; Yin et al. 2008a; Clark et al., 2010). Deformation in the Qaidam Basin and surrounding ranges accelerated in the early to middle Miocene (~20-15 Ma) (Chang et al., 2015; Yuan et al., 2013), accompanied by the uplift and sinistral movement of the Qimen Tagh-Eastern Kunlun range (Jolivet et al., 2003; Duvall et al., 2013) and the accelerated strike-slip motion along the Altyn Tagh Fault (Wu et al., 2012; Cheng et al., 2015). Growth strata from the seismic profiles show

331 synsedimentary deformation in the study area initiating in the middle to late Miocene
332 (15-8 Ma). Specifically, the Dafengshan, Jiandingshan, Jianbei, Changweiliang and
333 Jianshan anticlines began to develop at the start of Shangyoushashan Formation
334 (N_2^2sy, 15.3 Ma) deposition, and the Nanyishan, Xiaoliangshan and Heiliangzi
335 anticlines began to develop at the start of Shizigou Formation (N_2^3s, 8.1 Ma)
336 deposition (Fig. 3).
337 It is notable that no clear temporal pattern of fold growth is seen in the study area
338 of 70 km width (a-a' in Fig. 1). This calls into question the previous speculations by
339 Métivier et al. (1998), Yin et al. (2007, 2008b), Wu et al. (2013) and Wu et al. (2014b),
340 who described the northward or southward advance of deformation in the Qaidam
341 Basin. Further, expanding the reference range southward to the Kunbei fault system
342 and northward to the Lenghu structural belts (a distance of ca. 260km; b-b' in Fig. 1),
343 the initial times of growth of NW-trending structures are concentrated in the Miocene
344 (~20-8 Ma). From south to north, the onset of the Kunbei fault system was during the
345 early Miocene (Cheng et al., 2014; Cheng et al., 2015), the onset of the Yingxiongling
346 structure belts were during the middle Miocene (Yu et al., 2011), the onset of the
347 structures in our study area were during the middle Miocene, the onset of the Eboliang
348 structure belts were during the early-middle Miocene (Fu et al., 2009; Sun et al.,
349 2014), and the onset of the Lenghu structure belts were during the middle Miocene
350 (Wang et al., 2011). Therefore, we infer that most NW-trending structures in the
351 western Qaidam Basin have formed out of sequence since the early Miocene, though
352 deformation at the southern and northern margins of the Qaidam Basin commenced

somewhat earlier than in its interior parts.

Regional Tectonic Implications

This study identifies the subsurface structures of individual folds in the western Qaidam Basin as a series of sinistral positive flower structures (Fig. 7a). Clearly, these structures contribute to accommodating the convergence of the broad India-Eurasia collision zone.

One implication of our work is that the segmented, domal and discontinuous nature of the folds and underlying faults in the western Qaidam Basin does not support any direct connection between these structures and the Altyn Tagh Fault, as has been previously proposed (Meyer et al., 1998).

The distribution of earthquake focal mechanisms (Molnar and Lyon-Caen, 1989; Elliott et al., 2010; Global CMT calalog; Fig. 1) shows that seismic strain is not evenly distributed across the Qaidam Basin and adjacent mountain ranges. Much of the basin interior has little or no instrumental record of $M > 5$ earthquakes, contrasting with numerous thrust events at the basin margins. Strike-slip events are concentrated along the known strike-slip faults, including the Altyn Tagh, Haiyuan, Eastern Kunlun and Elashan faults. The orientation of the fold axes (Figs. 1 and 4a) and the sinistral slip sense of the structures (Figs. 5 and 6) within the Qaidam Basin are consistent with the oblique convergence recorded by GPS data across the basin and the mountain ranges to its north and south (Fig. 1; e.g. Gan et al., 2007; Liang et al., 2013). Whereas in those marginal ranges the strike-slip component of deformation is localized along single, large, sinistral strike-slip faults (Eastern Kunlun and Haiyuan

faults; i.e. strain partitioning, Fig. 7b), the oblique convergence within the western Qaidam Basin is distributed across the positive flower structures (Fig. 7a).

The differing deformation styles between the Qaidam Basin and the surrounding ranges may relate to the variable basement strength, and the resultant degree of shortening. The relatively rigid Precambrian basement of the Qaidam Basin has plausibly resisted Cenozoic deformation more successfully than the surrounding mountain ranges which were the loci of intense deformation during Paleozoic orogenies. We suggest that strain partitioning is more complete in these mountain ranges than that in the relatively stable, lower strain regions of the Qaidam Basin.

It is a further question why deformation is oblique across this part of the collision zone at all. A simple explanation is that there is at least partial extrusion of Eurasian lithosphere, eastwards, out of the path of the indenting Indian plate (Tapponnier et al., 2001) – and that the sinistral strike-slip faults within the Qaidam Basin are just a small component in this deformation. Zuza and Yin (2016) adopted the rotating crustal block models of England and Molnar (1990) and McKenzie and Jackson (1986). In this scenario, the sinistral faults rotate clockwise as they slip, permitting the western side of the system (e.g. the Tarim Basin) to move northwards with respect to the eastern side (e.g. eastern China - see Fig. 10 of Zuza and Yin, 2016). A third explanation was provided by England and Molnar (2005), who showed that the directions of horizontal compressional strain align with topographic gradients, and concluded that Eurasia deforms as a continuum under the influence of gravity. The implication of this conclusion is that where pre-existing structures are not perfectly

aligned to accommodate this strain, one of three scenarios can occur: creation of new structures, rapid rotation of pre-existing structures into the correct orientation, or strain partitioning of oblique convergence utilizing existing basement structures.

Our results do not allow us to discriminate completely between these different scenarios, which are not absolutely mutually exclusive. The structures do emphasise the continuum character of deformation, including the oblique component, which is at odds with any descriptions of extrusion tectonics that involve rigid, plate-like behavior (e.g. Avouac and Tapponnier, 1993). The deformation within the Qaidam Basin, with distributed strike-slip structures, seems to be different in style from the surrounding ranges. The overall kinematics are not distinctly different across the different regions, as revealed in the GPS data (Fig. 1).

CONCLUSIONS

The predominant structures in the western Qaidam Basin are a distributed array of NW-trending transpressive structures with sinistral strike-slip components. They display positive flower geometries in 2D seismic profiles and helicoidal shapes in 3D space. The branch faults in the sedimentary cover and the major faults in the basement are demonstrated by the high-quality seismic data. This kind of structural framework is different from the southern and northern basin-bounding ranges, where the efficient strain partitioning results in strike-slip deformation being localized on single, large sinistral faults (i.e. Eastern Kunlun and Haiyuan faults).

The initial activities of the transpressive structures in the study area started in the middle to late Miocene (15-8 Ma). These structures together with abundant other

NW-trending structures in the western Qaidam Basin show a randomness rather than a northward or southward propagation in the formation sequence, which indicates the uniform deformation within the Qaidam Basin has accelerated since the early Miocene.

The Qaidam Basin has a lower degree of strain compared with other regions of the Tibetan Plateau due to the higher strength of basement. However, it is clearly an over-simplification to treat the Qaidam Basin as a rigid block in the extrusion tectonic models. The pervasive transpressive structural deformation across the western Qaidam Basin is a plausible way to absorb the clockwise rotation which should have happened in the interior part of basin (Wang and Burchfiel, 2004), if fault block rotations models are correct (Zuza and Yin, 2016). The deformation mechanism is also consistent with regional compressive strain occurring at an oblique angle to basement faults, which are activated as sinistral flower structures in an example of distributed transpressional deformation.

APPENDIX

Mathematical equation set used in kinematic calculation of the faults in this paper:

$$V / \tan G1 - L = D1 \qquad (1)$$

$$V / \tan G2 + L = D2 \qquad (2)$$

Where *D1* and *D2* are the distances between the left two and right two reference points beside the fault respectively, *G1* and *G2* are the Gradients of the stratum in the left and right segments of the anticline respectively, and *L* and *V* are the lateral and

vertical offsets of the fault respectively (Table 1 and Fig. A1). *D1*, *D2*, *G1* and *G2* are known numbers in this equation set, which can be derived from the depth-structure maps, and *L* and *V* are unknown numbers which need to be worked out by the equation set. Note that, we assume the faults are nearly vertical in this calculation method.

ACKNOWLEDGMENTS

This work was funded by the National Science and Technology Major Project of China (2011E-03). We are grateful to Suotang Fu, Daowei Zhang, Dade Ma, Yunfa Feng, and Chuanwu Wang of Qinghai Oilfield Company for providing the seismic data in this paper. We also thank Wenjun Zhu, Anping Hou and Tailiang Jiang for their help in operating the seismic interpretation software.

REFERENCES CITED

Argand, E., 1924, La tectonique de l' Asie: 13th International Geological Congress Report Session, vol. 7, p. 171-372.

Avouac, J. P., and Tapponnier, P., 1993, Kinematic model of active deformation in Central Asia: Geophysical Research Letters, v. 20, p. 895-898, doi: 10.1029/93GL00128.

Beidinger, A., and Decker, K., 2011, 3D geometry and kinematics of the Lassee flower structure: Implications for segmentation and seismotectonics of the Vienna Basin strike-slip fault, Austria: Tectonophysics, v. 499, p. 22-40, doi: 10.1016/j.tecto.2010.11.006.

Chen, W., Chen, C., and Nábelek. J. L., 1999, Present-day deformation of the Qaidam basin with implications for intra-continental tectonics: Tectonophysics, v. 305, p. 165-181, doi: 10.1016/S0040-1951(99)00006-2.

Cheng, F., Jolivet, M., Fu S., Zhang, Q., Guan, S., Yu, X., and Guo, Z., 2014, Northward growth of the Qimen Tagh Range: A new model accounting for the Late Neogene strike-slip deformation of the SW Qaidam Basin: Tectonophysics, v. 632, p. 32-47, doi: 10.1016/j.tecto.2014.05.034.

Cheng, F., Guo, Z., Jenkins, H.S., Fu, S., and Cheng, X., 2015, Initial rupture and displacement on the Altyn Tagh fault, northern Tibetan Plateau: Constraints based on residual Mesozoic to Cenozoic strata in the western Qaidam Basin: Geosphere, v. 11, p. 921–942, doi:10.1130 /GES01070.1.

Cheng, X., Fu, S., Wang, H., Yu, X., Cheng, F., Liu, R., Du, W., and Guo, Z., 2015, Geometry and kinematics of the Arlar strike-slip fault, SW Qaidam basin, China: New insights from 3-D seismic data: Journal of Asian Earth Sciences. v. 98, p. 198–208, doi: 10.1016/j.jseaes.2014.09.039.

Clark, M. K., Farley, K. A., Zheng, D., Wang, Z., Duvall, A. R., 2010, Early Cenozoic faulting of the northern Tibetan Plateau margin from apatite (U-Th)/He ages: Earth and Planetary Science Letters, v. 296, p. 78-88, doi:10.1016/j.epsl.2010.04.051.

Dayem, K. E., Molnar, P., Clark, M. K., and Houseman G. A., 2009, Far-field lithospheric deformation in Tibet during continental collision: Tectonics, v. 28, TC6005, doi: 10.1029/2008TC002344.

485 Dupont-Nivet, G., Robinson, D., Butler, R. F., Yin, A., and Melosh, H. J., 2004,
486 Concentration of crustal displacement along a weak Altyn Tagh fault: Evidence
487 from paleomagnetism of the northern Tibetan Plateau: Tectonics, v. 23, TC1020,
488 doi: 10.1029/2002TC001397.
489 Duvall, A. R., and Clark, M. K., 2010, Dissipation of fast strike-slip faulting within
490 and beyond northeastern Tibet: Geology, v. 38, p. 223-226, doi:
491 10.1130/G30711.1.
492 Duvall, A. R., Clark, M. K., Kirby, E., Farley, K. A., Craddock, W. H., Li, C., and
493 Yuan, D., 2013, Low-temperature thermochronometry along the Kunlun and
494 Haiyuan Faults, NE Tibetan Plateau: Evidence for kinematic change during
495 late-stage orogenesis: Tectonics, v. 32, p. 1190-1211, doi:
496 10.1002/tect.20072,2013.
497 Elliott, J. R., Walters, R. J., England, P. C., Jackson, J. A., Li, Z., and Parsons, B.,
498 2010, Extension on the Tibetan plateau: recent normal faulting measured by
499 InSAR and body wave seismology: Geophysical Journal International, v. 183, p.
500 503-535, doi: 10.1111/j.1365-246X.2010.04754.x.
501 England, P., and Molnar, P., 1990, Right-lateral shear and rotation as the explanation
502 for strike-slip faulting in east Tibet: Nature, v. 344, p. 140-142, doi:
503 10.1038/344140a0.
504 England, P., and Molnar, P., 1997, Active deformation of Asia: From kinematics to
505 dynamics: Science, v. 278, p.647-650, doi: 10.1126/science.278.5338.647.

England, P., and Molnar, P., 2005, Late Quaternary to decadal velocity fields in Asia: Journal of Geophysical Research, v. 110, B12401, doi: 10.1029/2004JB003541.

Fang, X., Zhang, W., Meng, Q., Gao, J., Wang, X., King, J., Song, C., Dai, S., and Miao, Y., 2007, High-resolution magnetostratigraphy of the Neogene Huaitoutala section in the eastern Qaidam Basin on the NE Tibetan Plateau, Qinghai Province, China, and its implication on tectonic uplift of the NE Tibetan Plateau: Earth and Planetary Science Letters, v. 258, p. 293-306, doi:10.1016/j.epsl.2007.03.042.

Fu, S., Wang, L., Xu, Z., Ma, L., and Zhang, X., 2009, Geological conditions of deep gas pools and their favorable prospects: Natural Gas Geoscience, v. 20, p. 841-846 [in Chinese with English abstract].

Fu, S., Ma, D., Chen, Y., Wu, Z., Wang, Y., Hao, X., and Zhang, J., 2015, Natural gas exploration in eastern segment of Altyn piedmont, northern Qaidam Basin: China Petroleum exploration, v. 20, p. 1-13 [in Chinese with English abstract], doi: 10.3969/j.issn.1672-7703.2015.06.001.

Gan, W., Zhang, P., Shen, Z., Niu, Z., Wang, M., Wan, Y., Zhou, D., and Cheng, J., 2007, Present-day crustal motion within the Tibetan Plateau inferred from GPS measurements: Journal of Geophysical Research, v. 112, B08416, doi: 10.1029/2005JB004120.

Garzanti, E., Baud, A., and Mascle, G., 1987, Sedimentary record of the northward flight of India and its collision with Eurasia (Ladakh Himalaya, India): Geodinamica Acta, v. 1, p. 297-312, doi: 10.1080/09853111.1987.11105147.

Ge, X., Zhang, M., Liu, Y., Ye, H., and Shi, C., 1998, Scientific problems and thought for research of the Altyn Fault: Geoscience, v. 12, p. 295-301.

Gu, S., Xu, W., Xue, C., Di, S., Yang, F., Di, H., Zhao, D., 1990, Petroleum Geology of China Vol. 14: Oil Fields in Qianghai and Xizang: Beijing, Petroleum Industry Press, 483 p. [in Chinese].

Hao, G., Lu, S., Wang, H., Xin, H., and Li, H., 2004, The Pre-Devonian tectonic framework in the northern margin of Qaidam basin and geological evolution of Olongbuluck palaeo-block: Earth Science Frontiers, v. 11, p. 115-122 [in Chinese with English abstract].

Harding, T. P., 1990, Identification of wrench faults using subsurface structural data: Criteria and Pitfalls: American Association of Petroleum Geologists Bulletin, v. 74, p. 1590-1609, doi: 10.1306/0C9B2A29-1710-11D7-8645000102C1865D.

Huang, W., Dupont-Nivet, G., Lippert, P.C., van Hinsbergen, D.J.J., Dekkers, M.J., Guo, Z., Waldrip, R., Li, X., Zhang, X., Liu, D., and Kapp, P., 2015, Can a primary remanence be retrieved from partially remagnetized Eocence volcanics in the Nanmulin Basin (Southern Tibet) to date the India-Asia collision?: Journal of Geophysical Research: Solid Earth, v. 120, p. 42-66, doi: 110.1002/2014JB011599.

Jin, Z., and Zhang, B., 2006, The Geological Map of the Qaidam Basin: Qinghai Oilfield Company and China University of Petroleum-Beijing, scale 1: 1 000 000, 1 sheet [in Chinese].

549 Jin, Z., Zhang, M., Tang, L., and Li, J., 2004, Evolution of Meso-Cenozoic Qaidam
550 basin and its control on oil and gas: Oil and Gas Geology, v. 25, p. 603-608 [in
551 Chinese with English abstract].
552 Jolivet, M., Brunel, M., Seward, D., Xu, Z., Yang, J., Malavieille, J., Roger, F.,
553 Leyreloup, A., Arnaud, N., and Wu, C., 2003, Neogene extension and volcanism
554 in the Kunlun Fault Zone, northern Tibet: New constraints on the age of the
555 Kunlun Fault: Tectonics, v. 22, 1052, doi: 10.1029/2002TC001428,2003.
556 Jordan, T. A., and Watts, A. B., 2005, Gravity anomalies, flexure and the elastic
557 thickness structure of the India-Eurasia collisional system: Earth and Planetary
558 Science Letters, v. 236, p. 732-750, doi: 10.1016/j.epsl.2005.05.036.
559 Kapp, P., Pelletier, J.D., Rohrmann, A., Heermance, R., Russell, J., and Ding, L.,
560 2011, Wind erosion in the Qaidam basin, central Asia: implications for tectonics,
561 paleoclimate, and the source of the Loess Plateau: GSA Today, v. 21, p. 4-10,
562 doi: 10.1130/GSATG99A.1.
563 Ke, X., Ji, J., Zhang, K., Kou, X., Song, B., and Wang, C., 2013, Magnetostratigraphy
564 and anisotropy of magnetic susceptibility of the Lulehe Formation in the
565 northeastern Qaidam Basin: Acta Geologica Sinica-English Edition, v. 87, p.
566 576-587, doi: 10.1111/1755-6724.12069.
567 Li, Y., Zheng, Y., Xiong, X., and Hu, X., 2013, Lithospheric effective elastic
568 thickness and its anisotropy in the northeast Qinghai-Tibet plateau: Chinese
569 Journal of Geophysics, v. 56, p. 1132-1145 [in Chinese with English abstract],
570 doi: 10.6038/cjg20130409.

Liang, S., Gan, W., Shen, C., Xiao, G., Liu, J., Chen, W., Ding, X., and Zhou, D., 2013, Three-dimensional velocity field of present-day crustal motion of the Tibetan Plateau derived from GPS measurements: Journal of Geophysical Research, v. 118, p. 5755-5732, doi: 10.1002/2013JB010503.

Liu, Z., Wang, F., Liu, Y., Zhao, C., Gao, J., and Wang, C, 2009, Structural features and determination of deformation time in the Nanyishan-Jiandingshan area of Qaidam Basin: Journal of Jilin University (Earth Science Edition), v. 39, p. 796-802 [in Chinese with English abstract], doi: 10.13278/j.cnki.jjuese.2009.05.004.

Lu, H., and Xiong, S., 2009, Magnetostratigraphy of the Dahonggou section, northern Qaidam Basin, and its bearing on Cenozoic tectonic evolution of the Qilian Shan and Altyn Tagh fault: Earth and Planetary Science Letters, v. 288, p. 539-550, doi: 10.1016/j.epsl.2009.10.016.

Maltman, A., 1998, Geological Maps: An Introduction, 2nd Edition: John Wiley & Sons, 260 p.

Mao, L., Xiao, A., Zhang, H., Wu, Z., Wang, L., Shen, Y., and Wu, L., 2016, Structural deformation pattern within the NW Qaidam Basin in the Cenozoic era and its tectonic implications: Tectonophysics, v. 687, p. 78-93, doi: 10.1016/j.tecto.2016.09.008.

Mckenzie, D., and Jackson, J., 1986, A block model of distributed deformation by faulting: Journal of the Geological Society, London, v. 143, p. 349-353, doi: 10.1144/gsjgs.143.2.0349.

593 Meng, Q., and Fang, X., 2008, Cenozoic tectonic development of the Qaidam Basin in
594 the northeastern Tibetan Plateau: Geological Society of America Special Papers,
595 v. 444, p. 1-24, doi: 10.1130/2008.2444(01).
596 Métivier, F., Gaudemer, Y., Tapponnier, P., and Meyer, B., 1998, Northeastward
597 growth of the Tibet plateau deduced from balanced reconstruction of two
598 depositional areas: The Qaidam and Hexi Corridor basins, China: Tectonics, v.
599 17, p. 823-842, doi: 10.1029/98TC02764.
600 Meyer, B., Tapponnier, P., Bourjot, L., Métivier, F., Gaudemer, Y., Peltzer, G., Guo,
601 S., and Chen, Z., 1998, Crustal thickening in Gansu-Qinghai, lithospheric mantle
602 subduction, and oblique, strike-slip controlled growth of the Tibet plateau:
603 Geophysical Journal International, v. 135, p. 1-47, doi:
604 10.1046/j.1365-246X.1998.00567.x.
605 Molnar, P., and Tapponnier, P., 1975, Cenozoic tectonics of Asia: effects of a
606 continental collision: Science, v. 189, p. 419-426, doi:
607 10.1126/science.189.4201.419.
608 Molnar, P., and Lyon-Caen, H., 1989, Fault plane solutions of earthquakes and active
609 tectonics of the Tibetan Plateau and its margins: Geophysical Journal
610 International, v. 99, p.123-153, doi: 10.1111/j.1365-246X.1989.tb02020.x.
611 Pan, J., Li, H., Sun, Z., Liu, D., Wu, C., and Yu, C., 2015, Tectonic responses in the
612 Qaidam basin induced by Cenozoic activities of the Altyn Tagh fault: Acta
613 Petrologica Sinica, v. 31, p. 3701-3712 [in Chinese with English abstract].

614 Patriat, P., and Achache, J., 1984, India–Eurasia collision chronology has implications
615 for shortening and driving mechanism of plates: Nature, v. 311, p. 615-621, doi:
616 10.1038/311615a0.
617 Pei, J., Sun, Z., Wang, X., Zhao, Y., Ge, X., Guo, X., Li, H., and Si, J., 2009,
618 Evidence for Tibetan Plateau uplift in Qaidam Basin before Eocene-Oligocene
619 boundary and its climatic implications: Journal of Earth Science, v. 20, p.
620 430-437, doi: 10.1007/s12583-009-0035-y.
621 Qinghai Bureau of Geology and Mineral Resources (QBGMR), 1991, Regional
622 Geology of Qinghai Province: Beijing, Geological Publishing House, 662 p. [in
623 Chinese].
624 Rickard, M. J., 1971, A classification diagram for fold orientations: Geological
625 Magazine, v.108, p. 23-26.
626 Ritts, B.D., and Biffi, U., 2000, Magnitude of post-Middle Jurassic (Bajocian)
627 displacement on the central Altyn Tagh fault system, northwest China:
628 Geological Society of America Bulletin, v. 112, p. 61-74, doi:
629 10.1130/0016-7606(2000)112<61:MOPJBD>2.0.CO;2.
630 Rowley, D.B., 1996, Age of collision between India and Asia: a review of the
631 stratigraphic: Earth and Planetary Science Letters, v. 145, p. 1-13. doi:
632 10.1016/S0012-821X(96)00201-4.
633 Royden, L. H., Burchfiel, B. C., King, R. W., Wang, E., Chen, Z., Shen, F., and Liu
634 Y., 1997, Surface Deformation and Lower Crustal Flow in Eastern Tibet:
635 Science, v. 276, p. 788-790, doi: 10.1126/science.276.5313.788.

636 Shaw, J. H., Hook, S. C., and Suppe, J., 1994, Structural trend analysis by axial
637 surface mapping: American Association of Petroleum Geologists Bulletin, v. 78,
638 p. 700-721.
639 Shen, Z., Wang, M., Li, Y., Jackson, D. D., Yin, A., Dong, D., and Fang, P., 2001,
640 Crustal deformation along the Altyn Tagh fault system, western China, from
641 GPS: Journal of Geophysical Research: Solid Earth, v. 106, p. 30607-30621, doi:
642 10.1029/2001JB000349.
643 Song, T., and Wang, X., 1993, Structural styles and stratigraphic patterns of
644 syndepositional faults in a contractional setting: Examples from Qaidam Basin,
645 northwestern China: American Association of Petroleum Geologists Bulletin, v.
646 77, p. 102-117.
647 Sun, D., Duan, W., Deng, N., and Ying, S., 1956, The Qaidam vortex structure and its
648 tectonic significance: Acta Geologica Sinica, v. 36, p. 417-441 [in Chinese with
649 English abstract].
650 Sun, C., Qiao, Z., Yang, G., Zhang, H., Jing, M., Yang, F., and Sun, N., 2002,
651 Discussion on ownership of Qaidam Basin: Journal of Palaeogeography, v. 4, p.
652 59-66 [in Chinese with English abstract].
653 Sun, Z., Yang, Z., Pei, J., Ge, X., Wang, X., Yang, T., Li, W., and Yuan, S., 2005,
654 Magnetostratigraphy of Paleogene sediments from northern Qaidam Basin,
655 China: Implications for tectonic uplift and block rotation in northern Tibetan
656 Plateau: Earth and Planetary Science Letters, v. 237, p. 635-646, doi:
657 10.1016/j.epsl.2005.07.007.

Sun, Z., Jing, M., Sun, N., Lu, Y., and Cao, L., 2007, Discussion on boundary between the upper and lower members of Xiaganchaigou Formation of Paleogene in Well Kun-2, Qaidam Basin: Journal of Palaeogeography, v. 9, p. 611-618 [in Chinese with English abstract].

Sun, P., Wang, L., Guo, Z., Tian J., Zhang, L., Zeng, X., and Zhang, S., 2014, Oil and gas accumulation conditions of Eboliang structural belt on northern periphery of Qaidam Basin and exploration strategy: China Petroleum exploration, v. 19, p. 18-25 [in Chinese with English abstract], doi: 10.3969/j.issn.1672-7703.2014.04.003.

Sylvester, A. G., 1988. Strike-slip faults: Geological Society of America Bulletin, v. 100, p. 1666-1703, doi: 10.1130/0016-7606(1988)100<1666:SSF>2.3.CO;2.

Tapponnier, P., Xu, Z., Roger, F., Meyer, B., Arnaud, N., Wittlinger, G., and Yang, J., 2001, Oblique stepwise rise and growth of the Tibet Plateau: Science, v. 294, p. 1671-1677, doi: 10.1126/science.105978.

Wang, C., Gao, R., Yin, A., Wang, H., Zhang, Y., Guo, T., Li, Q., and Li, Y., 2011, A mid-crustal strain-transfer model for continental deformation: A new perspective from high-resolution deep seismic-reflection profiling across NE Tibet: Earth and Planetary Science Letters, v. 306, p. 279-288, doi: 10.1016/j.epsl.2011.04.010.

Wang, E., and Burchfiel, B. C., 2004, Late Cenozoic right-lateral movement along the Wenquan fault and associated deformation: Implications for the kinematic history of the Qaidam Basin, northeastern Tibetan Plateau: International Geology Review, v. 46, p. 861-879, doi: 10.2747/0020-6814.46.10.861.

Wang, E., Xu, F., Zhou, J., Wan, J., and Burchfiel, B.C., 2006, Eastward migration of the Qaidam Basin and its implications for Cenozoic evolution of the Altyn Tagh fault and associated river systems: Geological Society of America Bulletin, v. 118, p. 349-365, doi: 10.1130/B25778.1.

Wang, G., Ma, D., Zhang, Q., and Li, J., 2008, Basin-mountain tectonic pattern and hydrocarbon exploration domain in north margin of Qaidam Basin: Petroleum Exploration and Development, v. 35, p. 668-673 [in Chinese with English abstract].

Wang, G., Ma, D., Zhou, C., and Zhou, S., 2011, The seismic profile interpretation and development mechanism of strike-slip faults in northern Qaidam Basin: Acta Geoscientica Sinica, v. 32, p. 204-210 [in Chinese with English abstract], doi: 10.3975/cagsb.2011.02.09.

Wang, G., Wang, Q., Jian, P., and Zhu, Y., 2004, Zircon SHRIMP ages of Precambrian metamorphic basement rocks and their tectonic significance in the eastern Kunlun Mountains, Qinghai Province, China: Earth Science Frontiers, v. 11, p. 481-490 [in Chinese with English abstract].

Wang, M., 2003, The ‘thick top’ structure and its formation mechanism in Qaidam Basin: Xijiang Petroleum Geology, v. 24, p. 277-280 [in Chinese with English abstract].

Wang, Y., Zheng, J., Zhang, W., Li, S., Liu, X., Yang, X., and Liu, Y., 2012, Cenozoic uplift of the Tibetan Plateau: Evidence from the tectonic sedimentary

evolution of the western Qaidam Basin: Geoscience Frontiers, v. 3, p. 175-187, doi: 10.1016/j.gsf.2011.11.005.

Wei, G., Li Ben., Xiao A., Chen, H., Yang, S., 2005, Strike-thrust structures and petroleum exploration in northern Qaidam Basin, Earth Science Frontiers, 2005, v. 12, p. 397-402 [in Chinese with English abstract].

Woodcock, N. H., and Rickards, B., 2003, Transpressive duplex and flower structure: Dent Fault System, NW England: Journal of Structural Geology, v. 25, p. 1981-1992, doi: 10.1016/S0191-8141(03)00057-9.

Wu, C., Yan, C., Li, H., Tian, G., Sun, Z., Liu, D., Yu, C., and Pan, J., 2013, Cenozoic tectonic evolution of the western Qaidam Basin and its constrain on the growth of the northern Tibetan Plateau: Acta Petrologica Sinica, v. 29, p. 2211-2222 [in Chinese with English abstract].

Wu, G., Ge, X., Liu, Y., Yuan, S., Gong, Q., Chen, Y., and Shen, Y., 2006, Mesozoic-Cenozoic structural evolution in Qaidam Basin and its control on hydrocarbon occurrence: Global Geology, v. 25, p. 411-417 [in Chinese with English abstract].

Wu, L., Xiao, A., Yang, S., Wang, L., Mao, L., Wang, L., Dong, Y., and Xu, B., 2012, Two-stage evolution of the Altyn Tagh Fault during the Cenozoic: new insight from provenance analysis of a geological section in NW Qaidam Basin, NW China: Terra Nova, v. 24, p. 387-395, doi: 10.1111/j.1365-3121.2012.01077.x.

722 Wu, L., Xiao, A., and Yang, S., 2014a, Impact of wind erosion on detecting active
723 tectonics from geomorphic indexes in extremely arid areas: a case study from the
724 Hero Range, Qaidam Basin, NW China: Geomorphology, v. 224, p. 39-54, doi:
725 10.1016/j.geomorph.2014.07.010.
726 Wu, L., Xiao, A., Ma, D., Li, H., Xu, B., Shen, Y., and Mao, L., 2014b, Cenozoic
727 fault systems in southwest Qaidam Basin, northeastern Tibetan Plateau:
728 geometry, temporal development and significance for hydrocarbon accumulation:
729 American Association of Petroleum Geologists Bulletin, v. 98, p. 1213-1234, doi:
730 10 .1306 /11131313087.
731 Xia, W., Zhang, N., Yuan, X., Fan, L., and Zhang, B., 2001, Cenozoic Qaidam Basin,
732 China: A stronger tectonic inversed, extensional rifted basin: American
733 Association of Petroleum Geologists Bulletin, v. 85, p. 715-736, doi:
734 10.1306/8626C98D-173B-11D7-8645000102C1865D.
735 Xu, B., Xiao, A., Wu, L., Mao, L., Dong, Y., Jia, D., and Guan, J., 2013, Two-stage
736 activity of the Altyn Tagh Fault during the Cenozoic: Evidence from seismic
737 attributes analysis. Acta Petrologica Sinica, v. 29, p. 2859-2866 [in Chinese with
738 English abstract].
739 Xu, F., Yin, C., Gong, Q., and Shen, Y., 2006, Mesozoic-Cenozoic structural
740 evolution in Qaidam Basin and its control over oil and gas: China Petroleum
741 Exploration, v. 11, p. 9-16 [in Chinese with English abstract].

742 Yang, F., Ma, Z., Xu, T., and Ye, S., 1992, A Tertiary paleomagnetic stratigraphic
743 profile in Qaidam Basin: Acta Petrolei Sinica, v. 13, p. 97-101 [in Chinese with
744 English abstract].
745 Yin, A., and Harrison, T. M., 2000, Geologic evolution of the Himalayan-Tibetan
746 orogen: Annual Review of Earth and Planetary Sciences, v. 28, p. 211-280, doi:
747 10.1146/annurev .earth .28.1.211.
748 Yin, A., Rumelhart, P. E., Butler, R., Cowgill, E., Harrison, T. M., Foster, D. A.,
749 Ingersoll, R. V., Zhang, Q., Zhou, X., Wang, X., Hanson, A., and Raza, A., 2002,
750 Tectonic history of the Altyn Tagh fault system in northern Tibet inferred from
751 Cenozoic sedimentation: Geological Society of America Bulletin, v. 114, p.
752 1257-1295, doi:10.1130/0016-7606(2002)114<1257:THOTAT>2.0.CO;2.
753 Yin, A., Dang, Y., Zhang, M., McRivette, M.W., Burgess, W.P., and Chen, X., 2007,
754 Cenozoic tectonic evolution of Qaidam basin and its surrounding regions (part 2):
755 Wedge tectonics in southern Qaidam basin and the Eastern Kunlun Range:
756 Geological Society of America Special Paper, v. 433, p. 369–390, doi:
757 10.1130/2007.2433(18).
758 Yin, A., Dang, Y. Q., Wang, L. C., Jiang, W. M., Zhou, S. P., Chen, X. H., G. E.
759 Gehrels, and McRivette, M. W., 2008a, Cenozoic tectonic evolution of Qaidam
760 basin and its surrounding regions (Part 1): The southern Qilian Shan-Nan Shan
761 thrust belt and northern Qaidam basin: Geological Society of America Bulletin, v.
762 120, p. 813-846, doi: 10.1130.B26180.1.

763 Yin, A., Dang, Y., Zhang, M., Chen, X., and McRivette, M.W., 2008b, Cenozoic
764 tectonic evolution of the Qaidam Basin and its surrounding regions (Part 3):
765 Structural geology, sedimentation, and regional tectonic reconstruction:
766 Geological Society of America Bulletin, v. 120, p. 847-876,
767 doi:10.1130/B26232.1.
768 Yu, F., Wang, Y., Li, X., Li, X., and Feng, Z., 2011, Deformation characteristics and
769 genesis simulation of the Shizigou-Youshashan structural belt in Qaidamu Basin:
770 Geotectonica et Metallogenia, v. 35, p. 207-215 [in Chinese with English
771 abstract].
772 Yu, X., Huang, B., Guan, S., Fu, S., Cheng, F., Cheng, X., Zhang, T., and Guo, Z.,
773 2014, Anisotropy of magnetic susceptibility of Eocene and Miocene sediments in
774 the Qaidam Basin, Northwest China: Implication for Cenozoic tectonic transition
775 and depocenter migration: Geochemistry, Geophysics, Geosystems, v. 15, p.
776 2095-2108, doi: 10.1002/2014GC005231.
777 Yu, X., Guo Z., Jia C., and Fu S., 2016, A comparison of the landscape characters and
778 evolution of the huge basins around the Tibetan Plateau: Geotectonica et
779 Metallogenia (in press) [in Chinese with English abstract].
780 Yuan, D., Ge, W., Chen, Z., Li, C., Wang, Z., Zhang, H., Zhang, P., Zheng, D.,
781 Zheng, W., Craddock, W. H., Dayem, K. E., Duvall, A. R., Hough, B. G., Lease,
782 R. O., Champagnac, J. D., Burbank, D. W., Clark, M. K., Farley, K. A., Garzione,
783 C. N., Kirby, E., Molnar, P., and Roe, G. H., 2013, The growth of northeastern

784 Tibet and its relevance to large-scale continental geodynamics: A review of
785 recent studies: Tectonics, v. 32, p. 1358-1370, doi:10.1002/tect.20081.
786 Zeng, L., Jin, Z., Zhang, M., Tang, L., You, F., and Lei, B., 2002, The Jurassic basin
787 type and its evolution characteristic in Qaidam Basin: Acta Sedimentologica
788 Sinica, v. 20, p. 288-292, [in Chinese with English abstract], doi:
789 10.14027/j.cnki.cjxb.2002.02.017.
790 Zhai, G., Song, J., Jin, J., and Gao, W., 2002, Plate tectonic evolution and its
791 relationship to petroliferous basin: Beijing, Petroleum Industry Press, 461 p. [in
792 Chinese].
793 Zhang, W., Fang, X., Song, C., Appel, E., Yan, M., and Wang Y., 2013, Late
794 Neogene magnetostratigraphy in the western Qaidam Basin (NE Tibetan Plateau)
795 and its constraints on active tectonic uplift and progressive evolution of growth
796 strata: Tectonophysics, v. 599, p. 107-116, doi: 10.1016/j.tecto.2013.04.010.
797 Zhao, J., Tang, W., Li, Y., Yao, C., Zhang, J., Wang, W., and Huang, Y., 2006,
798 Lithospheric density and geomagnetic intensity in northeastern margin of the
799 Tibetan plateau and tectonic implications: Earth Science Frontiers, v. 13, p.
800 391-400 [in Chinese with English abstract].
801 Zhao, J., Jin, Z., Mooney, W. D., Okaya, N., Wang, S., Gao, X., Tang, L., Pei, S., Liu,
802 H., and Xu, Q., 2013, Crustal structure of the central Qaidam basin imaged by
803 seismic wide-angle reflection/refraction profiling: Tectonophysics, v. 584, p.
804 174-190, doi: 10.1016/j.tecto.2012.09.005.

805 Zheng, W., Zhang, P., Ge, W., Molnar, P., Zhang, H., Yuan, D., and Liu, J., 2013,
806 Late Quaternary slip rate of the South Heli Shan Fault (northern Hexi Corridor,
807 NW China) and its implications for northeastward growth of the Tibetan Plateau:
808 Tectonics, v. 32, p. 271-293, doi: 10.1002/tect.20022.
809 Zheng, Y., Mo, W., Zhang, W., and Guan, P., 2007, A new idea for petroleum
810 exploration in Qaidam Basin: Petroleum Exploration and Development, v. 34, p.
811 13-18 [in Chinese with English abstract].
812 Zhou, J., Xu, F., Wang, T., Cao, A., and Yin, C., 2006, Cenozoic deformation history
813 of the Qaidam Basin, NW China: Results from cross-section restoration and
814 implications for Qinghai-Tibet Plateau tectonics: Earth and Planetary Science
815 Letters, v. 243, p. 195-210, doi: 10.1016/j.epsl.2005.11.033.
816 Zhu, L., Owens, T. J., and Randall, G. E., 1995, Lateral variation in crustal structure
817 of the northern Tibetan Plateau inferred from teleseismic receiver functions:
818 Bulletin of the Seismological Society of America, v. 85, p.1531-1540.
819 Zhu, L., and Helmberger, D. V., 1998, Moho offset across the northern margin of the
820 Tibetan Plateau: Science, v. 281, p. 1170-1172, doi:
821 10.1126/science.281.5380.1170.
822 Zolnai, G., 1991, Continental wrench-tectonics and hydrocarbon habitat: tectonique
823 continentale en cisaillement: American Association of Petroleum Geologists
824 Continuing Education Course Notes Series, v. 30, p. 1-225, doi:
825 10.1306/CE30534.

826 Zuza, A. V., and Yin, A., 2016, Continental deformation accommodated by non-rigid
827 passive bookshelf faulting: An example from the Cenozoic tectonic development
828 of northern Tibet: Tectonophysics, v. 677-678, p. 227-240, doi:
829 10.1016/j.tecto.2016.04.007.

830

831 **FIGURE CAPTIONS**

832 Figure 1. Topography of the Qaidam Basin and surrounding regions. Inset: location of
833 the study area within the India-Eurasia collision zone. The GPS-derived velocities are
834 relative to stable Eurasia, from Gan et al. (2007). Black focal mechanisms are from
835 body wave modelling (Molnar and Lyon-Caen, 1989; Elliott et al., 2010), or the
836 Global CMT catalog where M >5.3 and there is >70% double couple. Grey focal
837 mechanisms are from the Global CMT catalog where M <5.3 and/or there is <70%
838 double couple.

839

840 Figure 2. (a) Geological map of the study area (Jin and Zhang, 2006), and locations of
841 the 2D seismic profiles, the two 3D seismic datasets and the two boreholes that are
842 used to reconstruct the subsurface structural framework. (b) Chronostratigraphic,
843 lithostratigraphic and seismic stratigraphic column of the Qaidam basin.

844

845 Figure 3. Seven selected seismic sections with detailed description in this paper.
846 Section A-A' crosses the Xiaoliangshan anticline. Section B-B' crosses the Nanyishan
847 anticline. The dashed line between the T4 and T6 seismic reflectors represent a

detachment unit in the Lower Xiaganchaigou Formation. Section C-C’ crosses the Jiandingshan anticline. Section D-D’ crosses the Dafengshan, the Heiliangzi and the Jianbei anticlines. Section E-E’ crosses the Dafengshan, the Heiliangzi and the Changweiliang anticlines. Section F-F’ crosses the Dafengshan and the Jianshan anticlines. VE: Vertical exaggeration. See Figure 4 for location.

Figure 4. (a) Synthetic map of faults traces (lines of intersection points) on the T1, T2′, T2, T4 and T6 seismic stratigraphic horizons. (b) Pseudo 3D model of the Dafengshan anticline. Note that the same colour lines in (a), (b) represent the same seismic reflectors.

Figure 5. Depth-structure maps of the Jiandingshan, the Nanyishan and the Dafengshan anticlines. NJF: the Northern Jiandingshan Fault; NNF: the Northern Nanyishan Fault; SDF: the Southern Dafengshan Fault. The reference contour lines show sinistral movement of the faults. Modified and redrawn from Qinghai Oilfield Company.

Figure 6. Remote sensing image of the western segment of the Nanyishan anticline, downloaded from Google Earth software with a pixel resolution of 1.19m. Three secondary faults near and subparallel to the boundary fault expose here and show sinistral strike-slip sense. See Figure 2 for location.

Figure 7. Schematic diagram of the deformation styles of (a) the Qaidam Basin (where oblique convergence is distributed across several transpressive structures), and (b) the Qilian Shan (where the strike-slip component appears to be localized along the Haiyuan Fault). The same overall convergence can be achieved by each configuration. The 3D model of the transpressive flower structure in (a) is modified from Woodcock & Rickards (2003); the postulated tectonic profile of the Qilian Shan in (b) is modified from Zheng et al. (2013).

Figure A1. Schematic of the geometric factors in the equation set used to calculate the lateral and vertical offsets of faults. Note that, the fault plane is assumed to be nearly vertical.

TABLE CAPTIONS

TABLE 1. GEOMETRIC DATA USED IN KINEMATIC CALCULATION OF THE THREE FAULTS IN FIGURE 5 AND THE RESULTS.

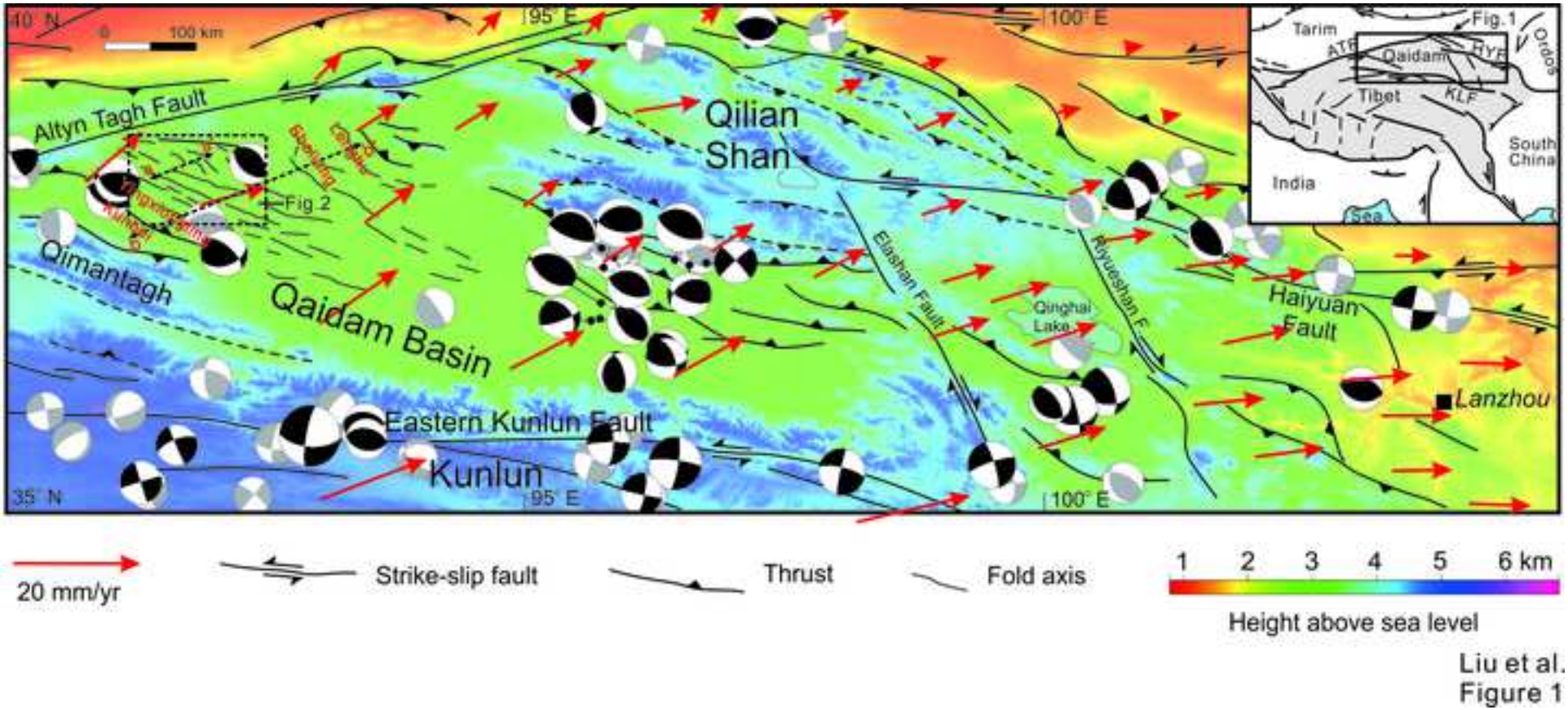

Liu et al.
Figure 1

Figure 2

Click here to download Figure Figure 2.jpg

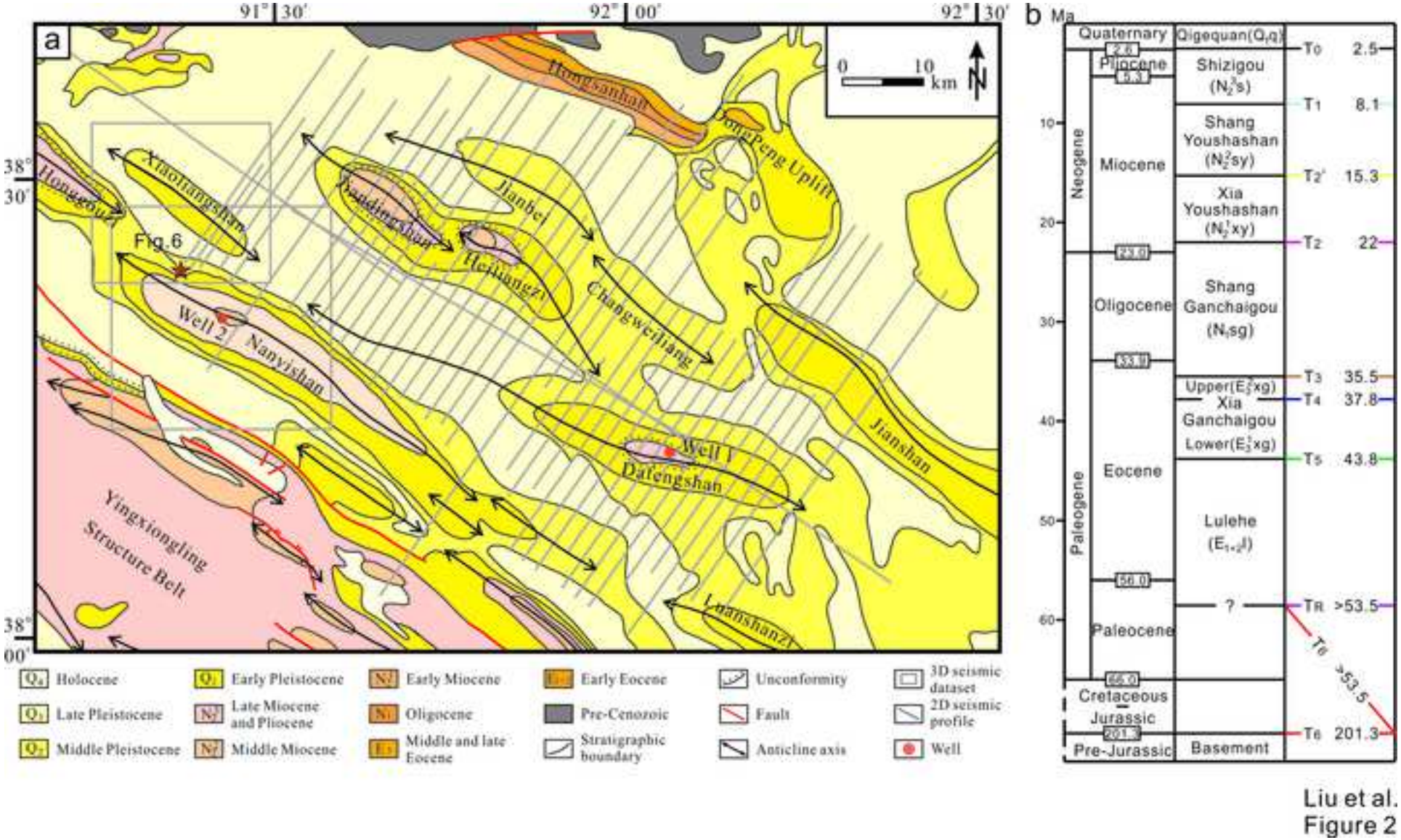

Liu et al.
Figure 2

Figure 3

Click here to download Figure Figure 3.jpg

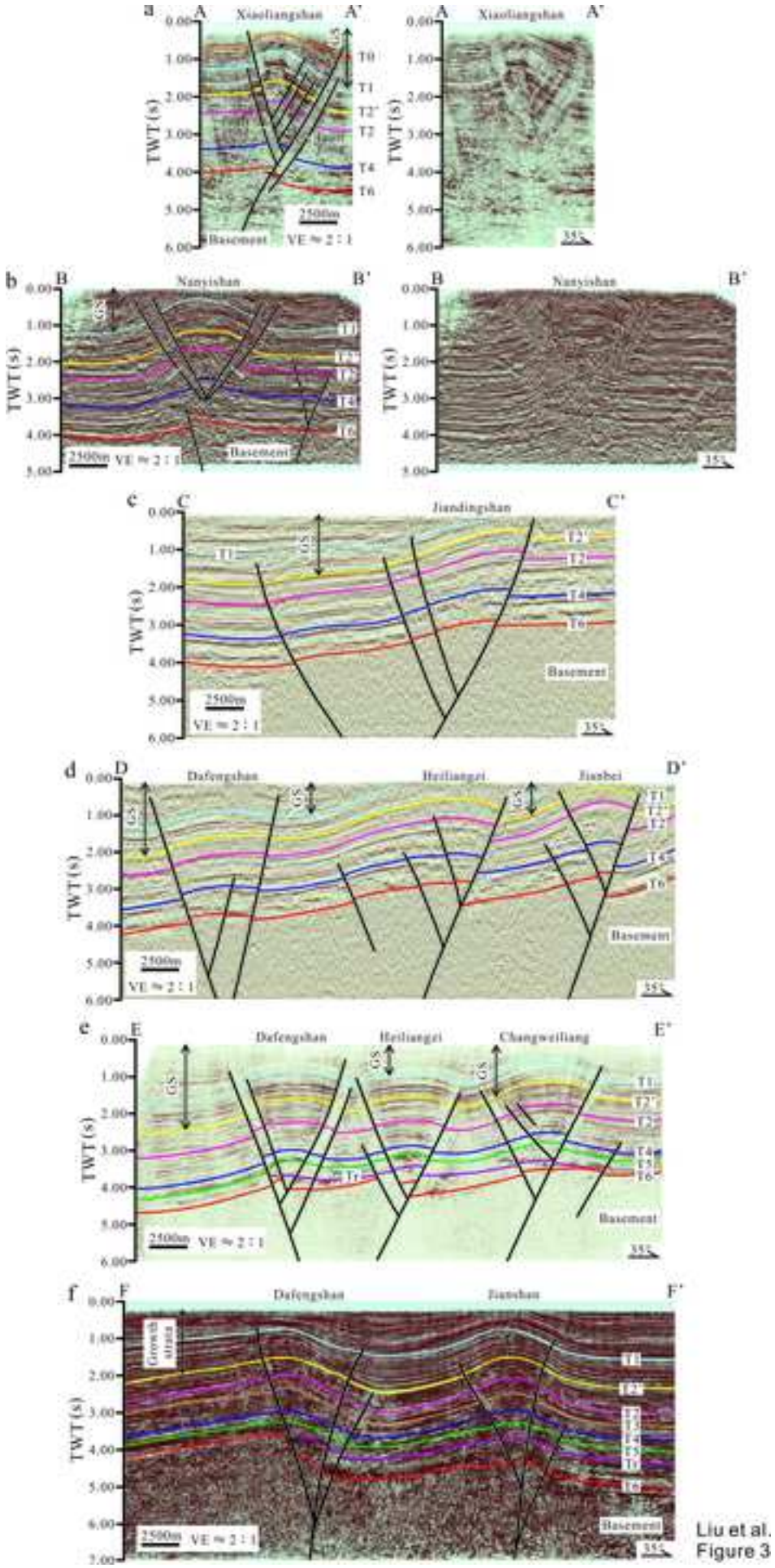

Liu et al.
Figure 3

Figure 4

Click here to download Figure Figure 4.jpg

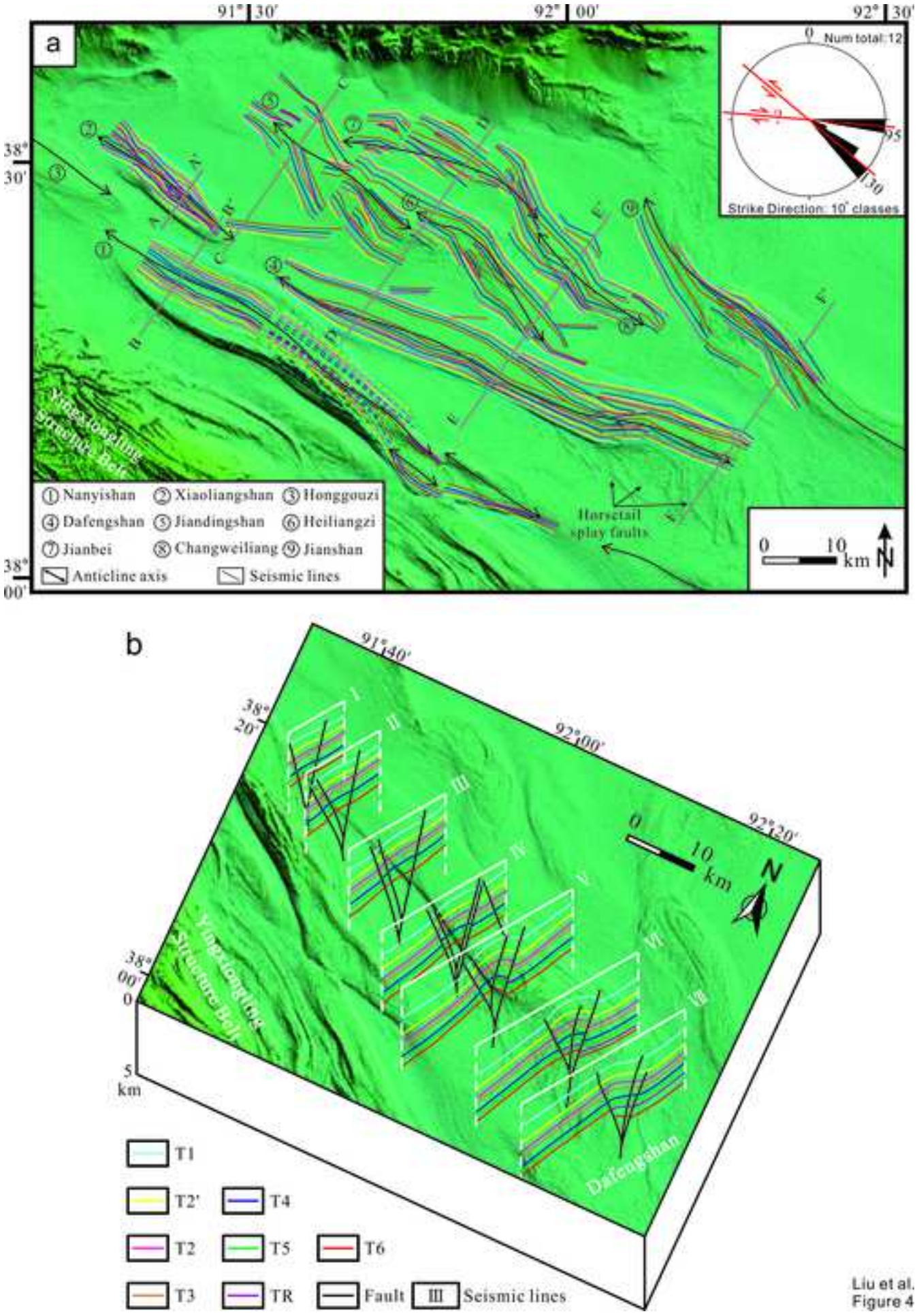

Liu et al.
Figure 4

Figure 5

Click here to download Figure Figure 5.jpg

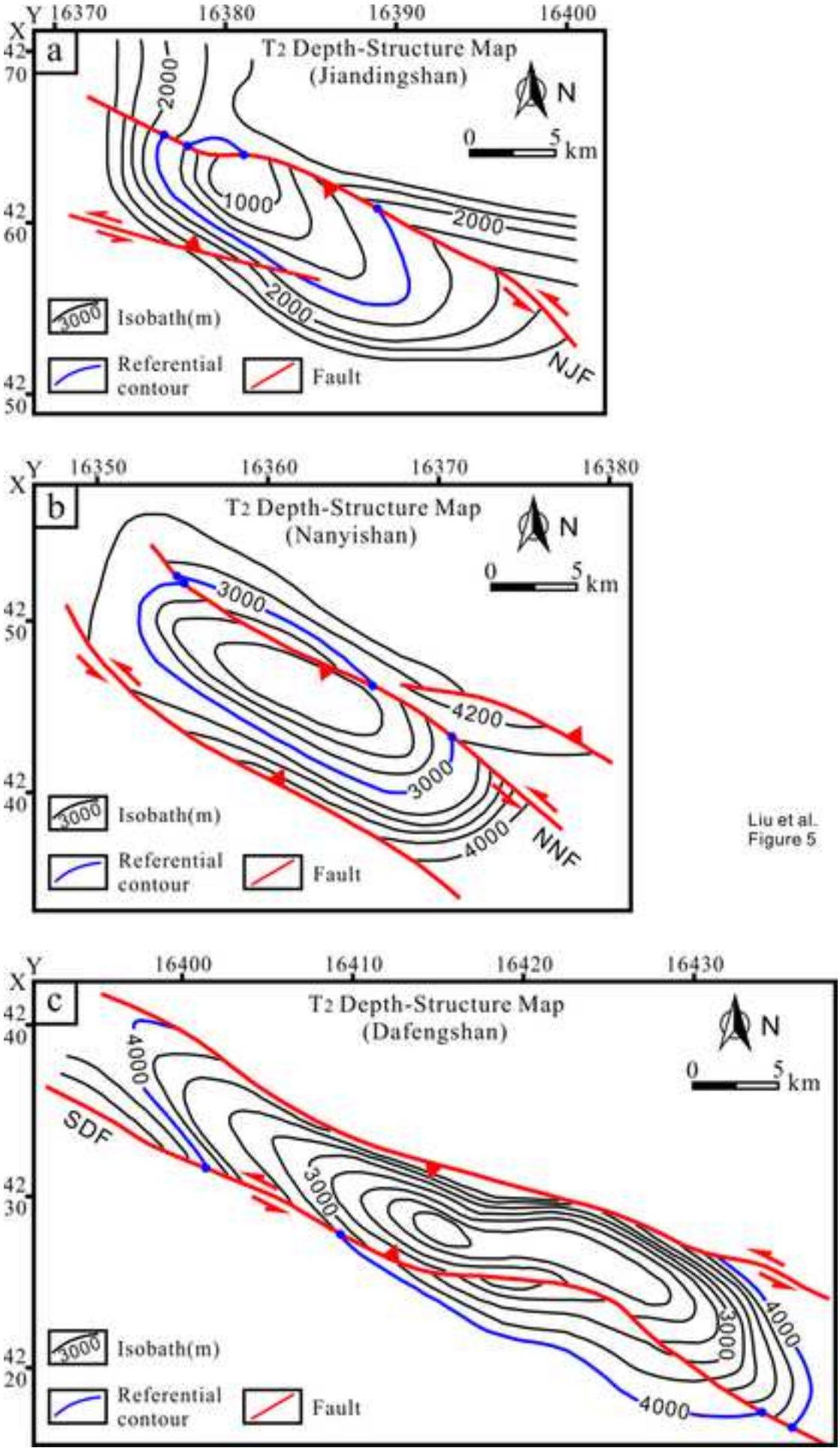

Liu et al.
Figure 5

Figure 6

Click here to download Figure Figure 6.jpg

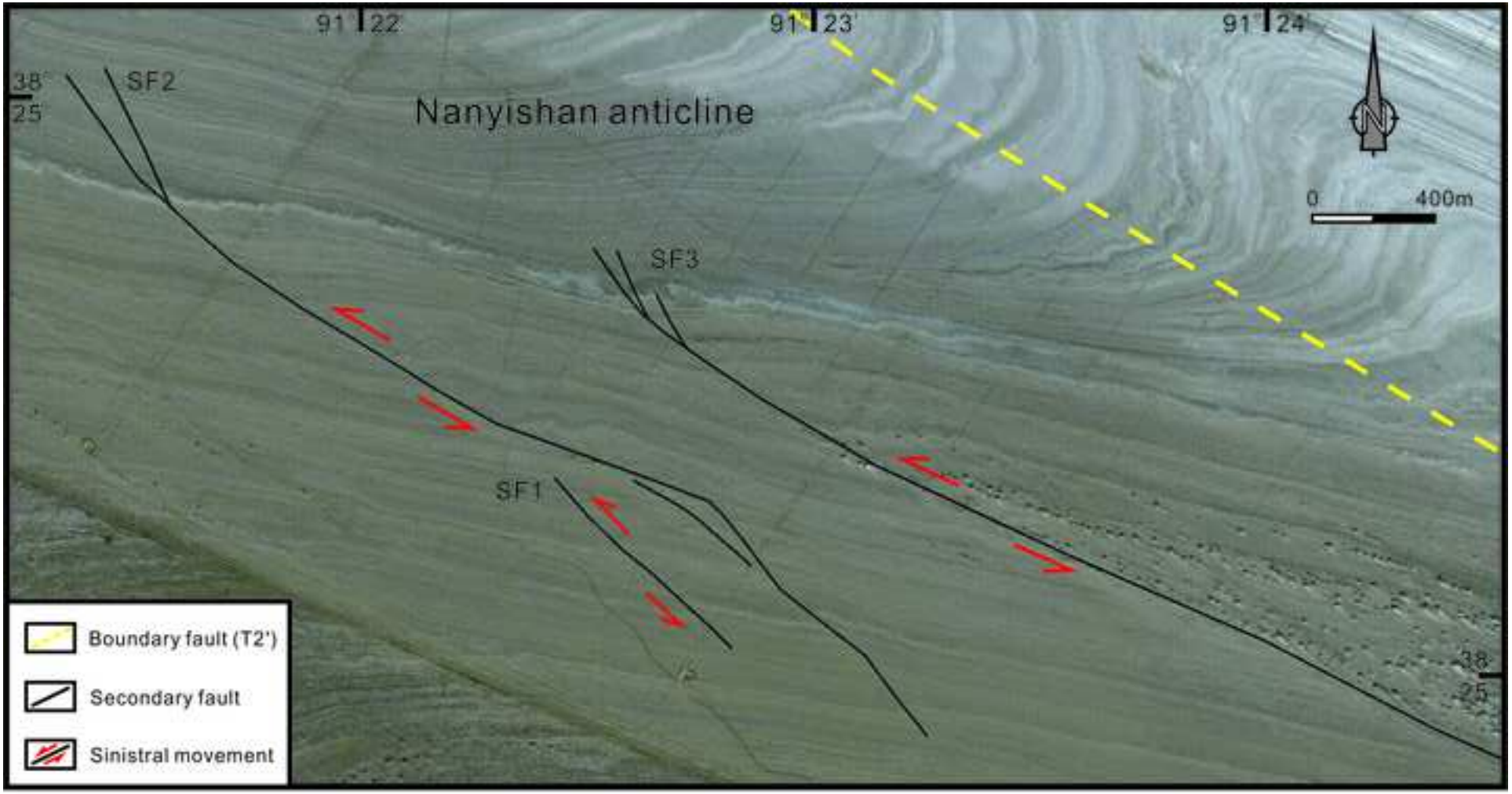

Liu et al.
Figure 6

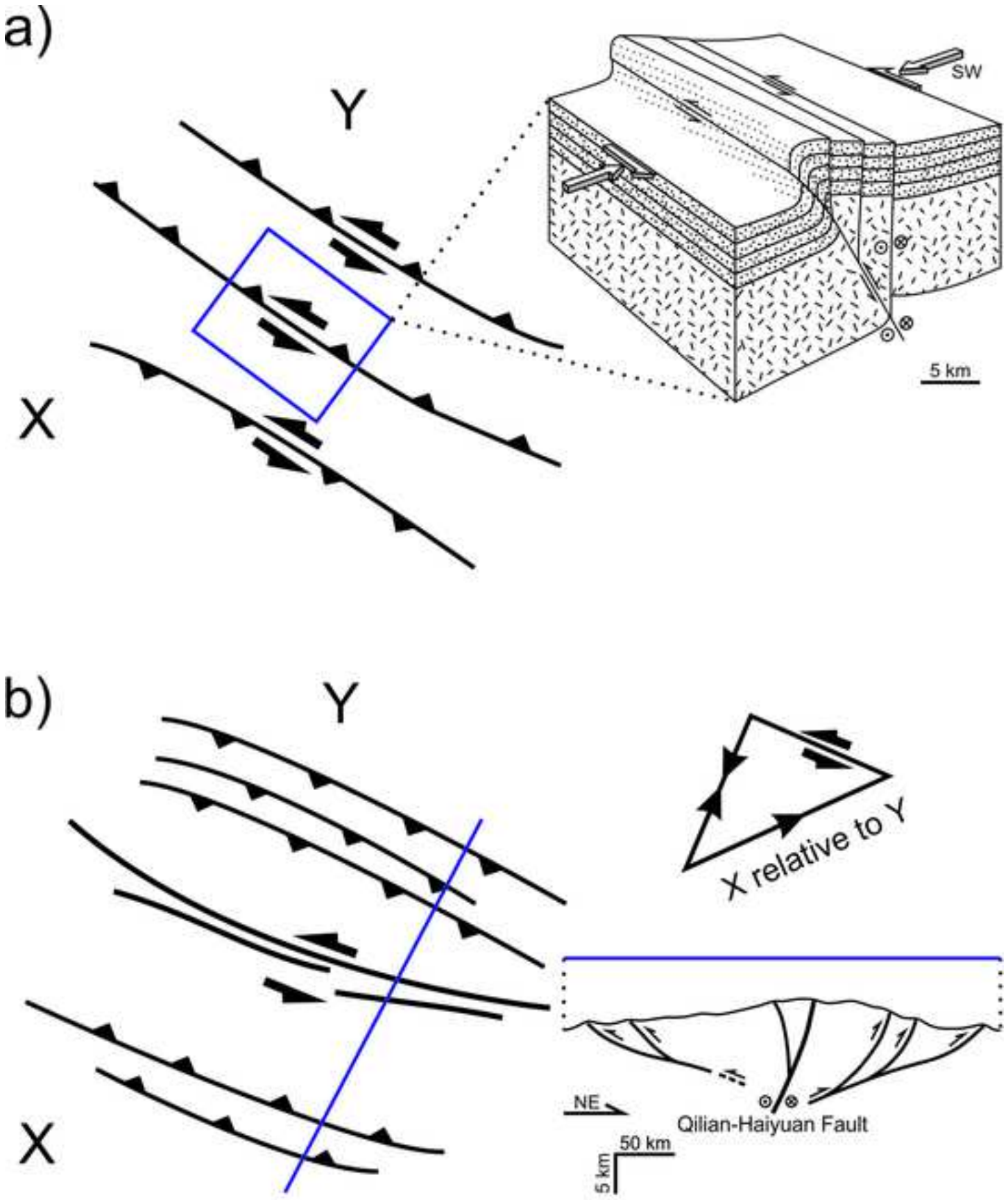

Table 1

TABLE 1. GEOMETRIC DATA USED IN KINEMATIC CALCULATION OF THE THREE FAULTS IN FIGURE 5 AND THE RESULTS

Fault name	Distance between the left two reference points (D1, km)	Distance between the right two reference points (D2, km)	Gradient of the stratum in the left (G1, °, parallel to the fault)	Gradient of the stratum in the right (G2, °, parallel to the fault)	Lateral offset (X, km)	Vertical offset (Y, km)
NJF	1.5	8.4	11.1	3.8	1.0	0.5
NNF	-1.2	5.5	5.6	6.2	3.5	0.2
SDF	8.8	2	5.4	7.8	2.4	0.6

* Sinistral: “+”; dextral: “-”; reverse: “+”, normal: “-”. Data in this table are acquired from Figure 5.

Supplemental material - Figure A1